Is it possible to quantify pebble abrasion and velocity in rivers using terrestrial cosmogenic nuclides?

Sébastien Carretier, V. Regard

Is it possible to quantify pebble abrasion and velocity in rivers using terrestrial cosmogenic nuclides?

S. Carretier[1,2] and V. Regard[1]

Received 18 January 2011; revised 14 July 2011; accepted 19 July 2011; published 15 October 2011.

[1] Attrition rates and mean transport velocities of coarse fluvial sediments averaged over long periods of time (≫100 a) are yet to be fully quantified. A knowledge of long-term transport rates would allow us to predict the response of fluvial systems to changes in external conditions, while determining clast attrition rates would improve our understanding of fluvial abrasion processes. The concentration of terrestrial cosmogenic nuclides (TCNs) in boulders can be modified during river transport by attrition and temporary exposure, which are two competing processes. In order to evaluate the potential of TCNs to quantify these processes, a stochastic model of TCN concentration evolution in clasts of different sizes is developed from exhumation on a hillslope to a sampling point in a river. The model includes shallow landslides or movement in a regolith and episodic transport of clasts in a sediment layer on the river bed. We study the downstream evolution of TCN concentrations for a population of clasts sourced from a localized TCN-rich lithology on a hillslope. When attrition is strong, the model predicts that the variance and maximum of TCN concentrations decrease downstream. Such a trend is possible only if the dominant hillslope erosion corresponds to shallow landslides. Natural variability of hillslope processes can hamper the trend. A way to limit the scatter is to sample the biggest clasts. On the contrary, if clast attrition is small and river transport slow, TCN concentrations increase downstream. In this case, combining the TCN concentrations of clasts gathered at several river stations should provide a method to estimate their mean transport rate. Our results offer guidelines to interpret the downstream evolution of TCN concentration in pebbles and at the surface of boulders.

Citation: Carretier, S., and V. Regard (2011), Is it possible to quantify pebble abrasion and velocity in rivers using terrestrial cosmogenic nuclides?, *J. Geophys. Res.*, *116*, F04003, doi:10.1029/2011JF001968.

1. Introduction

[2] The dynamics of sediment transport has been the focus of recent research efforts to understand the relationship between climate, tectonics and erosion. Sediment is considered as a first-order driver or inhibitor of bedrock channel erosion [e.g., *Attal and Lavé*, 2006; *Cowie et al.*, 2008; *Crosby et al.*, 2007; *Gasparini et al.*, 2006; *Lague*, 2010; *Sklar and Dietrich*, 2004, 2006; *Turowski et al.*, 2007; *Whipple and Tucker*, 2002]. Moreover, sediment transport rates determine river geomorphology and the response time of rivers to changes in sediment production, climate or tectonics [*Castelltort and van den Driessche*, 2003; *Church*, 2006; *Hovius et al.*, 2000; *Stark et al.*, 2009].

[3] The erosion rate of the river bedrock depends on the size and velocity of the clasts impacting it [*Sklar and Dietrich*, 2001; *Whipple et al.*, 2000; *Sklar and Dietrich*, 2004; *Sklar et al.*, 2008]. The grain size distribution of transported sediment can vary downstream either by selective transport and deposition, or by clast abrasion [e.g., *Paola et al.*, 1992a; *Attal and Lavé*, 2006, 2009, and references therein]. The relative influence of these processes in downstream sediment fining in rivers is still a matter of debate [e.g., *Attal and Lavé*, 2006; *Brewer and Lewin*, 1993; *Chatanantavet et al.*, 2010; *Knighton*, 1982; *Paola et al.*, 1992b]. It seems essential to define a method to quantify attrition rate independently of sorting due to selective deposition [*Attal and Lavé*, 2006, 2009].

[4] At the same time, our knowledge of coarse sediment mean velocities in rivers, averaged over long time periods (≫100 a) or large distances (≫1 km), is incomplete. This shortcoming prevents the testing of long-term fluvial erosion and transport laws. For example, it has been suggested, based on sedimentological records and physical and theoretical models, that large alluvial rivers behave like diffusive systems that buffer high-frequency sediment production variations [e.g., *Allen*, 2008; *Carretier and Lucazeau*, 2005; *Castelltort and van den Driessche*, 2003; *Metivier and Gaudemer*, 1999; *Metivier et al.*, 1999; *Paola et al.*, 1992a]. Determining the response time of alluvial systems is fundamental to analyzing

[1]GET, UPS (SVT-OMP), Université de Toulouse, Toulouse, France.
[2]IRD, GET, UPS (SVT-OMP), Université de Toulouse, Toulouse, France.

0148-0227/11/2011JF001968

stratigraphic records in terms of tectonic or climatic variations in the source catchments [*Castelltort and van den Driessche*, 2003]. Nevertheless, with a few exceptions [e.g., *Dosseto et al.*, 2006; *Granet et al.*, 2007], there is still a lack of data for long-term sediment transport rates in rivers that would allow us to test the diffusive nature of sediment transport. In addition, the transport distance of a clast population is thought to control the development of river bed instabilities such as dunes, bars and meanders [e.g., *Church*, 2006; *Charru*, 2006; *Davy and Lague*, 2009; *Pyrce and Ashmore*, 2003]. In large rivers, the characteristic time necessary to develop instabilities may be longer than the time period over which bed load rates are usually measured (several years or less).

[5] Classical bed load measurement methods are based on local measurement (using the Helley-Smith sampler for example) or tagged bed load clast displacements [e.g., *Ferguson et al.*, 1996]. Both methods are difficult to carry out in rivers with strong discharge variability and large clasts [*Liu et al.*, 2008; *Pyrce and Ashmore*, 2003; *Vericat et al.*, 2006]. Moreover, the period of measurement may not cover the entire range of hydrological events that contribute to progressive bed load sediment movement [*Pyrce and Ashmore*, 2003], possibly missing the contribution of large events [*Kirchner et al.*, 2001]. New integrative methods allow sediment transport rates to be averaged over long time spans (>1000 a). These methods are based either on the disequilibrium between the uranium series nuclides or on terrestrial cosmogenic nuclides (TCN) [e.g., *Chabaux et al.*, 2006; *Nichols et al.*, 2002; *Vigier et al.*, 2001]. They have been used to quantify the sediment transport rates in large alluvial systems such as the Ganges plain [*Chabaux et al.*, 2006; *Granet et al.*, 2007], the Amazon plain [*Dosseto et al.*, 2006; *Wittmann et al.*, 2009] and piedmonts in the Mojave Desert [*Nichols et al.*, 2002]. So far these methods have been applied to sand only; long-term transport rates of pebbles (2–6 cm diameter), cobbles (6–20 cm diameter) and boulders (20 cm-1 m diameter) have yet to be quantified.

[6] In a recent theoretical study, we investigated the relationship between clast size, clast velocity and TCN concentration for pebbles [*Carretier et al.*, 2009a]. In parallel, a field study showed that the TCN concentration in pebbles can be modified during fluvial transport [*Belmont et al.*, 2007]. Other studies showed significant differences in TCN concentration between sand and pebbles in river deposits [*Oskin et al.*, 2008]. *Carretier et al.'s* [2009a] results suggested that the downstream TCN concentration in clasts could fill the above mentioned gap by providing, in some cases, a tool to quantify both a clast attrition rate and a mean velocity or transport distance of clasts over millennia. However, the conclusions were preliminary, in particular because TCN concentration evaluations were valid for small pebbles only.

[7] In this paper, we expand the theory to pebbles and larger clasts to evaluate the possibility of quantifying clast abrasion and long-term mean velocity from the TCN concentrations at clast surfaces. In particular, we aim to evaluate the possible limits of this method and to establish a suitable sampling strategy.

2. Theoretical Basis

[8] A clast (boulder to sand) is assumed to go through three stages of evolution, the first one during its residence on the hillslope, the second during its residence on hillslopes and the third during its transport in the river (Figures 1 and 3). TCN production decreases at depth, so a concentration gradient develops within big clasts during the different stages. *Vassallo et al.* [2007] showed an example of different ^{10}Be concentrations at opposite points of a boulders on the hillslope of a Gobi Altay mountain. During its transport on the hillslope and in the river, the clast can roll and a radial gradient can eventually develop inside: on average TCN production at the boulder surface is greater than at boulder center, but the TCN concentration at the clast surface is heterogeneous. Then, two end-member scenarios can be imagined during river transport (Figure 1). The first one corresponds to significant erosion of the clast surface (attrition) and low TCN acquisition during fluvial transport. In this case, both the maximum TCN concentration and the variance of TCN concentrations within the clast can decrease downstream (Figure 1a). The second, on the contrary, is related to low clast attrition and slow river transport. In this case, TCN concentrations can increase within the clast [*Nichols et al.*, 2002] (Figure 1b). This simple idea may be the basis for a quantification method of attrition rate and/or river transport mean velocity.

[9] However, many natural or technical factors are likely to introduce clast-to-clast variability:

[10] 1. Hillslope processes are neither constant nor homogeneous.

[11] 2. The TCN-rich lithology can cover a significant range of altitudes and thus of TCN production rates on hillslopes.

[12] 3. Clasts produced on hillslopes have different sizes and shapes.

[13] 4. The transport in the river is stochastic.

[14] 5. Sampling a clast depends on its size: a piece of the surface for boulders, a piece or the whole surface for cobbles, the entire clast for pebbles.

[15] To avoid such complications due to natural variability it is necessary to take into account a population of clasts. These potential sources of variability raise three questions investigated in this paper: (1) What is the range of parameters that produce either a decrease (attrition) or an increase (river transport) of TCN concentration during river transport? (2) Does this signal surpass the natural variability of TCN concentration and apply to a population of clasts? (3) If it does, what is the best sampling strategy?

[16] The study is limited to the case of a unique TCN-rich lithological source in a catchment, so that clast provenance can be identified in the river. This restriction avoids the problem of the mixing of different sources at confluences which would prevent any simple interpretation of downstream TCN concentration evolution in terms of attrition or river transport [*Binnie et al.*, 2006; *Carretier et al.*, 2009b].

3. A Transport-TCN Concentration Model for One Clast

[17] In order to answer these three questions, we have developed a clast-scale TCN acquisition model based on pioneering work by *Repka et al.* [1997] and quite similar to the particle-based model of *Codilean et al.* [2010]. Our model, adapted from *Carretier et al.* [2009b], differs from previous models [*Granger et al.*, 1996; *Nichols et al.*, 2002;

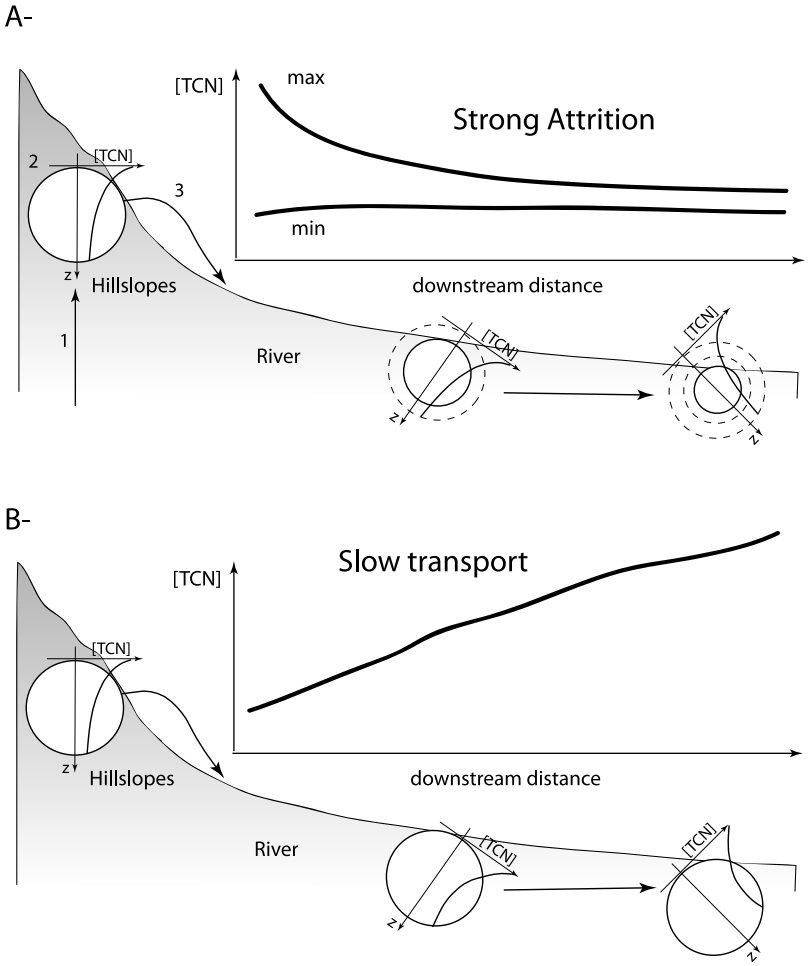

Figure 1. Conceptual model for the downstream evolution of TCN concentrations ([TCN]) at the clast surface. During exhumation on hillslopes, a TCN concentration gradient develops within the clast. During river transport, two end-member scenarios can be considered for the downstream evolution of TCN concentrations at the clast surface. (a) The clast size decreases rapidly and the TCN concentrations within the clast do no change significantly during river transport because it is rapid or because the clast travels at depth in the alluvial bed. In this case, the variance and maximum of the TCN concentrations decrease downstream. (b) The clast size does not vary and the river transport is sufficiently long for TCN concentrations to increase downstream.

Wittmann et al., 2009; *Yanites et al.*, 2009] by computing TCN concentration variations in clasts of different sizes (from boulder to sand). It is a 2D model (distance along the clast path, elevation). The upper part of the topographic profile is linear and corresponds to the hillslope. The lower part is a classical logarithmic (concave) river profile [e.g., *Whipple and Tucker*, 1999].

[18] The evolution of the TCN concentration N [$\mathcal{N}$/M] for any point inside a clast is given by the equation

$$\frac{dN}{dt} = -\lambda N + P(t) \tag{1}$$

where λ is the radioactive decay rate [T^{-1}] and P(t) is the TCN production rate [$\mathcal{N}$/M/T] at any time t. The production rate depends on the clast location on Earth, elevation and depth. All three vary during exhumation and transport because the clast rolls at the surface, is trapped at depth and travels downstream over large distances.

[19] Clasts are assumed spherical and always buried. Only the top of the clast can reach the surface (see Figure 2). Shielding effects associated with topographic slope [*Lal and Chen*, 2005] are not taken into account (discussed later).

[20] The TCN concentration is calculated at several points of a given clast (Figure 4a): (1) at the center, (2) the mean concentration at the clast surface ("Mean"), (3) the bulk TCN concentration, and (4) at two diametrically opposed points ("Top" and "Bottom") located initially along the vertical axis of the clast during the first stage of exhumation on hillslope ("1" in Figure 3). In order to calculate the mean clast surface TCN concentration, the clast is divided into concentric layers. For each layer within the clast, an average TCN concentration can be calculated that holds whether the clast rolls or not (Appendix A). The mean

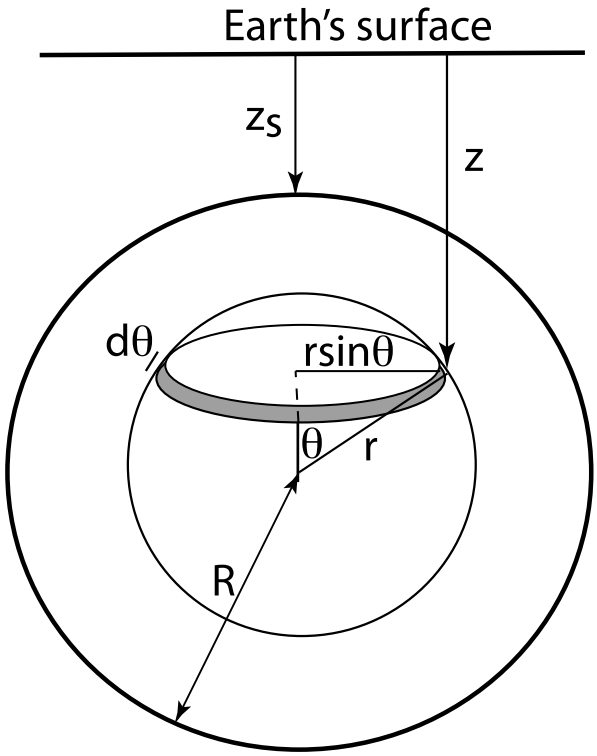

Figure 2. Characteristics of a clast of radius R at a depth z_s from the Earth's surface used to calculate a mean TCN concentration on a layer of radius r.

TCN concentration is calculated using a mean production rate P_r for each layer of radius r in a clast of radius R, the top of which is at a depth z_s (see Appendix A and Figure 2):

$$P_r = F_r\, e^{-z_s/\mu}\, P_s \tag{2}$$

where μ is an attenuation length [L] associated with a particle (neutron, fast muon, slow muon), P_s the production rate at the Earth's surface and F_r is a scale factor depending on R and r (see Appendix A). Then we calculate the TCN evolution of each layer by solving equation (1) with $P = \sum P_r$ (the sum of the different contributing particles), where R, z_s and P_s vary with time. μ depends on material density, which is taken to be constant in this study.

3.1. TCN Acquisition on Hillslope

[21] A hillslope is defined by its length, relief and maximum elevation. A clast can be exhumed anywhere on a hillslope. Two hillslope models are considered (Figure 3). Model 1 corresponds to shallow landslides ("shallow" meaning that the thickest landslide layer corresponds to the biggest clast diameter- 1m in this study), while Model 2 corresponds to a diffusion of clasts in a regolith layer, including the possibility that clasts could be removed from the surface to simulate soil-wash losses. We derive analytical solutions for the TCN concentration acquisition on the hillslope for the two models.

3.1.1. Model 1 (Shallow Landslides)

[22] A clast is progressively exhumed (stage 1 in Figure 3) until it becomes part of a landslide layer that will collapse. In order to compute the TCN concentration of a given clast, we have to specify probability functions for clast depth and its residence time in the landslide layer, the latter being the time elapsed since the previous landslide. Recent studies have shown that landslide sizes are distributed either as power laws or truncated double Pareto functions [e.g., *Hovius et al.*, 1997; *Stark and Hovius*, 2001; *Guzzetti et al.*, 2002; *Stark and Guzzetti*, 2009; *Larsen et al.*, 2010]. Landslide occurrence has been considered to be a Poisson process with landslides independent of one another [e.g., *Guzzetti et al.*, 2006; *Yanites et al.*, 2009]. A recent study pointed out the possible time clustering of landslides [*Witt et al.*, 2010]. Considering a clast of a given size, its probability to move with a landslide, its probability to be at a given depth and its residence time depend on landslide occurrence and size probabilities, and also on the clast-size distribution within the landslide layer (itself dependent on a fracture model). Combining these probabilities to reproduce the clast-size-dependent distribution of TCN concentrations on the hillslope is not straight-forward. We simplify the problem by choosing the depth of the clast top in the landslide layer randomly between 0 and a maximum H-2R (where H is the landslide thickness) and by assuming that the clast residence time T_h obeys a Gaussian distribution. Although this model does not allow the investigation of a large range of clast generation processes, it predicts a large range of clast-to-clast TCN concentration variations, which is our objective here. We want to test how the initial scatter in TCN concentrations is able to hamper the downstream signal obtained with a single clast. The possible effects of other probability distributions for the clast depth and residence time are discussed further in section 5.1. A mean T_h corresponds to the time needed to erode a layer of thickness H with a specified mean long-term erosion rate ϵ_h. The standard deviation of the Gaussian distribution is T_h/4, which produces a large range of residence times mainly distributed between 0 and 2T_h.

[23] In a natural case dominated by landslides, the exhumation is episodic (stage 1). However, it is approximated by a continuous rise of the clast toward the surface in the model. This approximation is valid if most of the investigated clast-to-clast variability in TCN concentrations is due to different residence depths and times in the landslide layer. When the clast becomes part of the landslide layer, the average TCN concentration on the clast layer is approximated by a secular steady state concentration:

$$N = \frac{P_s F_r}{\lambda + \epsilon_h/\mu}\, e^{-z/\mu} \tag{3}$$

where P_s is the TCN production rate at the Earth's surface, F_r the scale factor calculated in Appendix A, R is the clast radius, λ the radioactive decay constant, and μ the attenuation length for spallation. TCN concentrations at clast top and bottom are obtained for z and $z = (z + 2R)$, respectively, with $F_r = 1$ (no depth averaging).

[24] Then when the clast leaves the hillslope, the mean TCN concentration in a clast layer is given by:

$$N = F_r P_s \left[\frac{e^{-\lambda T_h}}{\lambda + \epsilon_h/\mu}\, e^{-z/\mu} + \frac{\left(1 - e^{-\lambda T_h}\right)}{\lambda}\, e^{-z/\mu} \right) \Bigg] \tag{4}$$

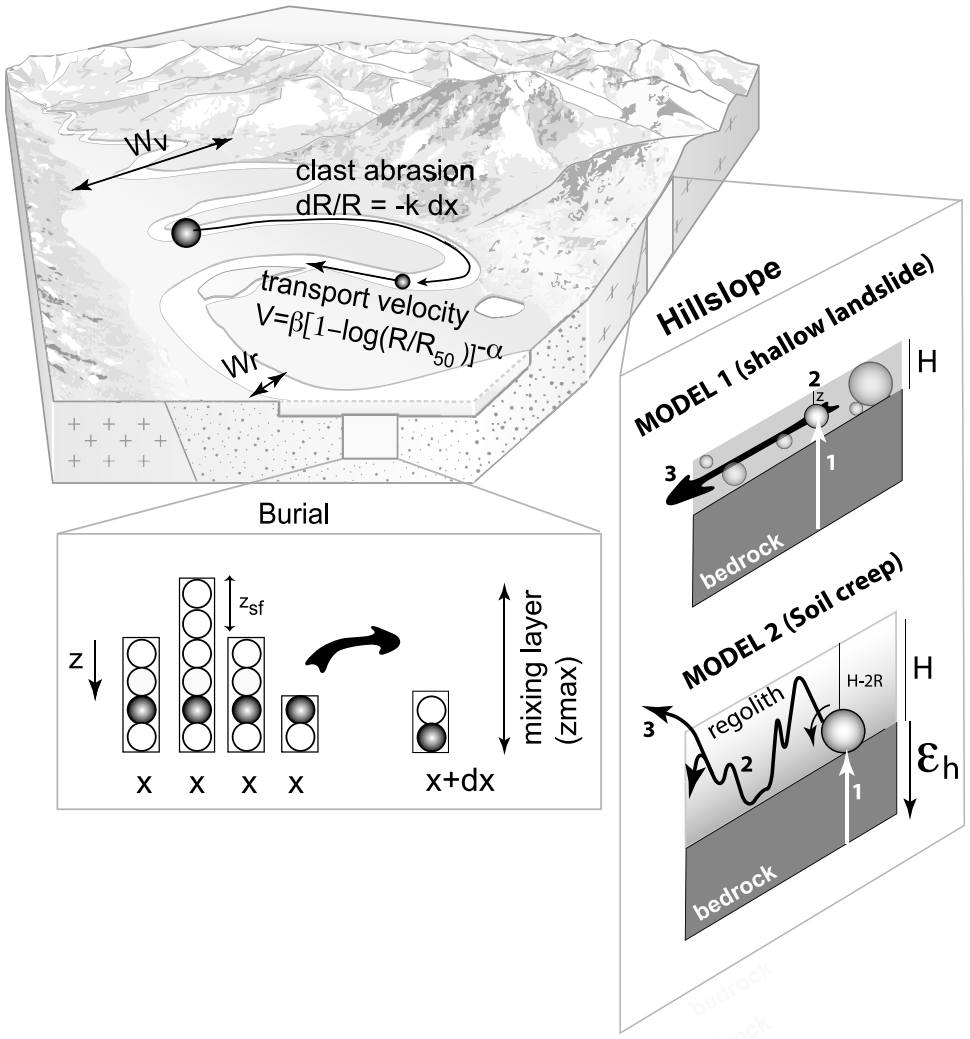

Figure 3. Model illustration. On hillslopes, TCNs accumulate during exhumation, detachment from the bedrock and residence at the hillslope surface. In Model 1 (shallow landslide) the clast depth is randomly positioned between 0 and H-2R. H is the maximum landslide layer thickness and R is the clast radius. The clast residence time in this layer is random with a mean defined by H/ϵ_h, ϵ_h being the long term erosion rate. In Model 2 (movement in a regolith), once detached, the clast migrates into a regolith of constant thickness H, developing at a constant rate ϵ_h. The mean residence time in the regolith depends on the location where it becomes part of the regolith. Gaussian variations are added to this mean. When buried in the river alluvium, the depth of the black clast varies with the addition/removal of overlying sediment and the duration of transport. For a time span integrating many hydrological events, the maximum range of river bed surface variations defines the mixing layer thickness, which is imposed as a model parameter. The burial depth is stochastic and depends on the ratio between the mixing layer thickness and a characteristic scour-deposit thickness z_{sf} for each hydrological event. When the clast is at the bed surface, it is transported at a velocity inversely dependent on the radius. The probability that the clast is in the river bed or in the adjacent terrace depends on the ratio between the valley width W_v and the active river width W_r. Attrition rate: k [L^{-1}], clast velocity: V [LT^{-1}]. Modified from *Carretier et al.* [2009b], with permission from Elsevier.

where T_h and z are chosen randomly within a Gaussian distribution. For clarity, only the spallation contribution to production rate is written, but muonic contributions are taken into account in the model using the proportionality coefficients and attenuation lengths of *Braucher et al.* [2003] (Table 1).

3.1.2. Model 2 (Movement in a Regolith)

[25] It is assumed that the Earth's surface erodes at a constant rate ϵ_h [L/T] on hillslopes. There is a concomitant development of a regolith, with a constant thickness H reflecting an equilibrium between erosion and weathering [*Small et al.*, 1999] (Figure 3). Once the regolith layer reaches

Table 1. Model Parameters[a]

Parameter	Definition
[L], [T], [M], [$\mathcal{N}$]	dimensions of length, time, mass, number of atoms
β [L T^{-1}]	clast velocity law factor (1 km/a)
ϵ_h [L T^{-1}]	hillslope erosion rate (0.01 mm/a)
F_r [1]	scaling factor used to calculate the mean TCN prod. rate at clast surface
H [L]	maximum landslide thickness or regolith thickness (1 m)
k [L^{-1}]	clast attrition rate (5%/km)
N [$\mathcal{N}$ M^{-1}]	cosmogenic nuclide concentration
P_o [$\mathcal{N}$ M^{-1}T^{-1}]	production rate at Earth's surface
μ_1 [L] = 0.6 m	depth attenuation for neutrons
μ_2 [L] = 6 m	depth attenuation for slow muon
μ_3 [L] = 21.2 m	depth attenuation for fast muon
λ [T^{-1}] = 4.62E-7 a^{-1}	radioactive decay for ^{10}Be
R [L]	clast radius
R_{50} [L]	Median radius of the mixture (7 cm)
t	travel time in river
V [LT^{-1}]	clast velocity
$\overline{V}(t)$ [L T^{-1}]	time-averaged clast velocity
Wr	river width
Wv	valley width
χ_1 = 0.9785	contribution of neutron spallation to total prod. rate at the surface
χ_2 = 0.015	contribution of slow muon capture to total prod. rate at the surface
χ_3 = 0.0065	contribution of fast muon-induced reactions to prod. rate at the surface
$z_{\max}$ [L]	mixing layer thickness (1 m)
z_{sf} [L]	characteristic scour-fill thickness (10 cm)

[a]Parameters of cosmogenic production rate are from *Stone* [2000] and *Braucher et al.* [2003]. Values in brackets are those of the reference model.

the base of a clast (of specified radius R), this clast is detached from the bedrock and transported downhill in the regolith layer. The regolith is vertically mixed: clast paths are assumed random in this layer, with an equal probability for the clast top to exist at all depths between the regolith surface and the regolith depth minus the clast diameter (H-2R). A resulting average TCN concentration can be calculated for a clast [e.g., *Granger et al.*, 1996; *Small et al.*, 1999]. Random variations around this mean are incorporated by adding variations to the mean residence time on hillslope. These variations can simulate sudden evacuation by surface wash, shorter or longer residence related to stochastic diffusive transport in the regolith [*Heimsath et al.*, 2002], or variations in regolith thickness. These variations are assumed to obey a Gaussian distribution in order to make the comparison with Model 1 easier. Analytical solutions of TCN concentrations within clasts are obtained by summing those processes. Those solutions neglect the decrease in production rate when the clast travels downhill.

[26] The TCN concentration for a concentric layer of radius r in a clast of radius R corresponds to the sum of the initial secular exhumation (stage 1) and the residence in the regolith (stage 2) [*Granger et al.*, 1996]:

$$N = F_r P_s \left[\frac{e^{-\lambda T_h}}{\lambda + \epsilon_h/\mu} e^{-(H-2R)/\mu} + \mu \frac{\left(1 - e^{-\lambda T_h}\right)}{\lambda} \frac{\left(1 - e^{-(H-2R)/\mu}\right)}{H - 2R} \right] \quad (5)$$

where T_h is the residence time in the regolith. The first term of the sum corresponds to the secular exhumation. The second term containing (H-2R) results from the integral of the TCN production rate P_r between 0 and H-2R, namely the possible range of clast top depths (z_s in equation (2)) during its movement within the regolith.

[27] A mean T_h can be established by balancing the hillslope outflux $U(d)H$ ($U(d)$ is the clast velocity at a distance d from hilltop) and the material influx in the regolith ϵ_h d. For a clast becoming part of the regolith at a distance d from the hilltop, T_h is

$$T_h = \int_d^{L_h} \frac{\mathrm{d}d'}{U(d')} \quad (6)$$

where L_h is the hillslope length. This leads to

$$T_h = \frac{H}{\epsilon_h} \ln\left(\frac{L_h}{d}\right), \quad d > 0 \quad (7)$$

T_h is much larger for a clast produced near the hilltop than for a clast produced at the foot of the hill, because $U(d)$ increases downslope. Furthermore, Gaussian perturbations are added to T_h with a standard deviation of T_h/4.

[28] For the TCN concentration at clast "Top",

$$N = P_s \left[\frac{e^{-\lambda T_h}}{\lambda + \epsilon_h/\mu} e^{-(H-2R)/\mu} + F_r \mu \frac{\left(1 - e^{-\lambda T_h}\right)}{\lambda} \frac{\left(1 - e^{-(H-2R)/\mu}\right)}{H - 2R} \right] \quad (8)$$

and at clast "Bottom",

$$N = P_s \left[\frac{e^{-\lambda T_h}}{\lambda + \epsilon_h/\mu} e^{-H/\mu} + F_r \mu \frac{\left(1 - e^{-\lambda T_h}\right)}{\lambda} \frac{\left(1 - e^{-(H-2R)/\mu}\right)}{H - 2R} \right] \quad (9)$$

Note that the second term is similar for "Top" and "Bottom" and that the scaling factor F_r is applied in both cases (Appendix A). This term corresponds to the integration of all the positions that those two points can take within the regolith while the clast is rolling. In this model, the TCN concentration polarity is acquired mainly during exhumation (stage 1), whereas in model 1, it forms during exhumation and residence in the landslide layer.

[29] Note that models 1 and 2 give the same result on average at the clast surface (for non-random T_h) if they share the same H and ϵ_h, if the clast diameter is H, and if the exhumation point of the clast is located at $d = 0.37L_h$ (leading to identical T_h in both models).

3.2. TCN Acquisition in the River

[30] The modeling approach is different for river transport. Equation (1) is solved numerically by time increment for each clast layer rather than by establishing analytical solutions. This method takes into account the downstream change in production, transport and clast erosion rates along the river. Since those parameters change non-linearly with the travel distance, analytical solutions are not straightforward.

[31] The clast can move if it is at the river bed surface. Otherwise, it can be trapped in a mixing layer or in a terrace (Figure 3). The mixing layer is subdivided into slices of

characteristic scour and fill thickness z_{sf}. A clast has a probability $z_{sf}/z_{\max}$ to lie in any slice of river bed. It can move if it is in the surface layer, which means that it has a probability $z_{sf}/z_{\max}$ to move. At depth, two competing effects are possible in the mixing layer: (1) an increase of TCN concentration due to a long stay close to the surface, and (2) a decrease in TCN concentration by radioactive decay if the clast is deeply buried.

[32] In the same way, a clast can reside in the active channel or in terraces. The probability that the clast is in the channel is given by the ratio of the channel width W_r to the valley width W_v: W_r/W_v (Figure 3). The presence of terraces ($W_v > W_r$) increases the clast residence time in the fluvial system and adds fluctuations to TCN concentrations.

[33] The transport length of a clast is the product of the time step and a relationship for velocity V [L T^{-1}] depending on the clast radius R:

$$V = \beta\left(1 - \log_{10}\frac{R}{R_{50}}\right)^{1.35} \tag{10}$$

where β [L/T] is the transport velocity of clasts of median size (R_{50}). This law is based on the distribution of pebble transport distances in gravel bed rivers [*Church and Hassan*, 1992]. Whether this law may be generally applicable or not, it allows us to take into account a possible difference in clast travel length based on clast size [*Ferguson and Wathen*, 1998], a component of fractional transport [e.g., *Hill et al.*, 2010; *Malmaeus and Hassan*, 2002; *Wilcock*, 1997]. The difference disappears when R is close to R_{50}, because the moving clasts interact with river bed roughness [e.g., *Malmaeus and Hassan*, 2002].

[34] Note that the mean transport velocity averaged over many increments of time tends toward:

$$\overline{V} = \frac{z_{sf}}{z_{\max}}\frac{W_r}{W_v}V \tag{11}$$

However, small clasts traveling rapidly over long distances may not experience all depths of the mixing layer during their stay in the river. Over a given period of time, this behavior yields differences in the mean hop lengths of clasts with a small but significant probability that clasts travel large distances. For these clasts, the mean transport velocity (and residence time in river) can deviate significantly from equation (11), compared to clasts that travel shorter distances. This process is a source of TCN concentration differences between clasts.

[35] During transport, clasts undergo abrasion. Therefore, their radius decreases at a rate k [L^{-1}]:

$$R(x) = R_O e^{-k\,x} \tag{12}$$

a form of the commonly used Sternberg's law [e.g., *Attal and Lavé*, 2006]. R_o is the initial clast radius. x is the distance from its injection point into the river. The clast is initially divided into 100 concentric layers. Each time the clast moves, a new radius is calculated using equation (12). If the erosion abrades the surface layer of the clast completely, the underlying layer becomes the new surface layer and so on. Note that in our model, k does not vary with the residence time in a terrace or river. Our model thus does not replicate clast weakening by weathering during storage [*Jones and Humphrey*, 1997].

[36] The attrition rate k [L^{-1}] should not be confused with the clast erosion rate [L/T]. The exponential form of the radius decrease (equation (12)) implies that the clast erosion rate [L/T] is not constant downstream. This rate depends not only on the attrition rate but also on clast velocity (for details see *Carretier et al.* [2009b]).

[37] To sum up, the clast starts with TCN concentrations calculated on hillslope using equations (4)–(9). Then TCN concentrations are calculated by time increments of 0.5 year along the river using equation (1).

4. Results

[38] In order to quantify the relative importance of the range of parameters that modify TCN concentrations in a clast, we have designed a basic reference model from which model parameters will be modified. The model corresponds to a drainage basin with a TCN-rich source at the catchment head, allowing the same lithological source to be identified and sampled all along the river. This TCN-rich lithological source extends 500 m horizontally and 500 m vertically on the hillslope. The river profile is logarithmic, 100 km long downstream with 2 km of vertical relief and the outlet located at 1750 m.a.s.l. Such a geometry is common in many mountain ranges, such as the Andes. For example, the river Aroma in northern Chile fits this geometry and includes a unique source of Paleozoic gneiss located in the catchment [*Farias et al.*, 2005].

[39] The tested hillslope model 1 corresponds to shallow landslides with a maximum landslide thickness of 1 m. Long-term hillslope mean erosion rate ϵ_h is 0.5 mm/a. The mixing layer $z_{\max}$ is 1 m thick in the river bed, which is about two times the attenuation length of neutrons (~0.6 m). The scour-fill thickness z_{sf} is 20 cm. The river width equals the valley width (no terrace, $\frac{W_r}{W_v} = 1$); $z_{\max}$, z_{sf} and $\frac{W_r}{W_v}$ are constant downstream. The relationship for transport velocity corresponds to a median grain size of $R_{50} = 7$ cm with a velocity of $\beta = 1$ km/a. The attrition rate is $k = 5\%$/km, which is an upper limit value for the most common rock types [*Attal and Lavé*, 2009]. This value was exceeded only by some highly friable schists and poorly cemented sandstone in the experiments of *Attal and Lavé* [2009].

[40] For an initial clast radius of 0.5 m, those parameters lead to an average residence time of 2000 a on the hillslope and 500 a in the river with a final clast radius of 2 cm after a 60 km travel distance. Given this rapid river transport and strong attrition rate, the reference model favors the attrition signal in the TCN concentrations compared to the signal associated with a long residence time in the river. The TCN investigated is ^{21}Ne (stable) with a production rate at sea level and midlatitudes of 21 at/g/a in quartz [*Gosse and Phillips*, 2001].

4.1. Reference Model

[41] Figure 4b shows the downstream evolution of the TCN concentration at different points (defined on Figure 4a and its caption) of a boulder 0.5 m in radius, exhumed initially in the middle of the hillslope.

[42] The first observation is that TCN concentration decreases at the "Top" and increases at the "Bottom." The

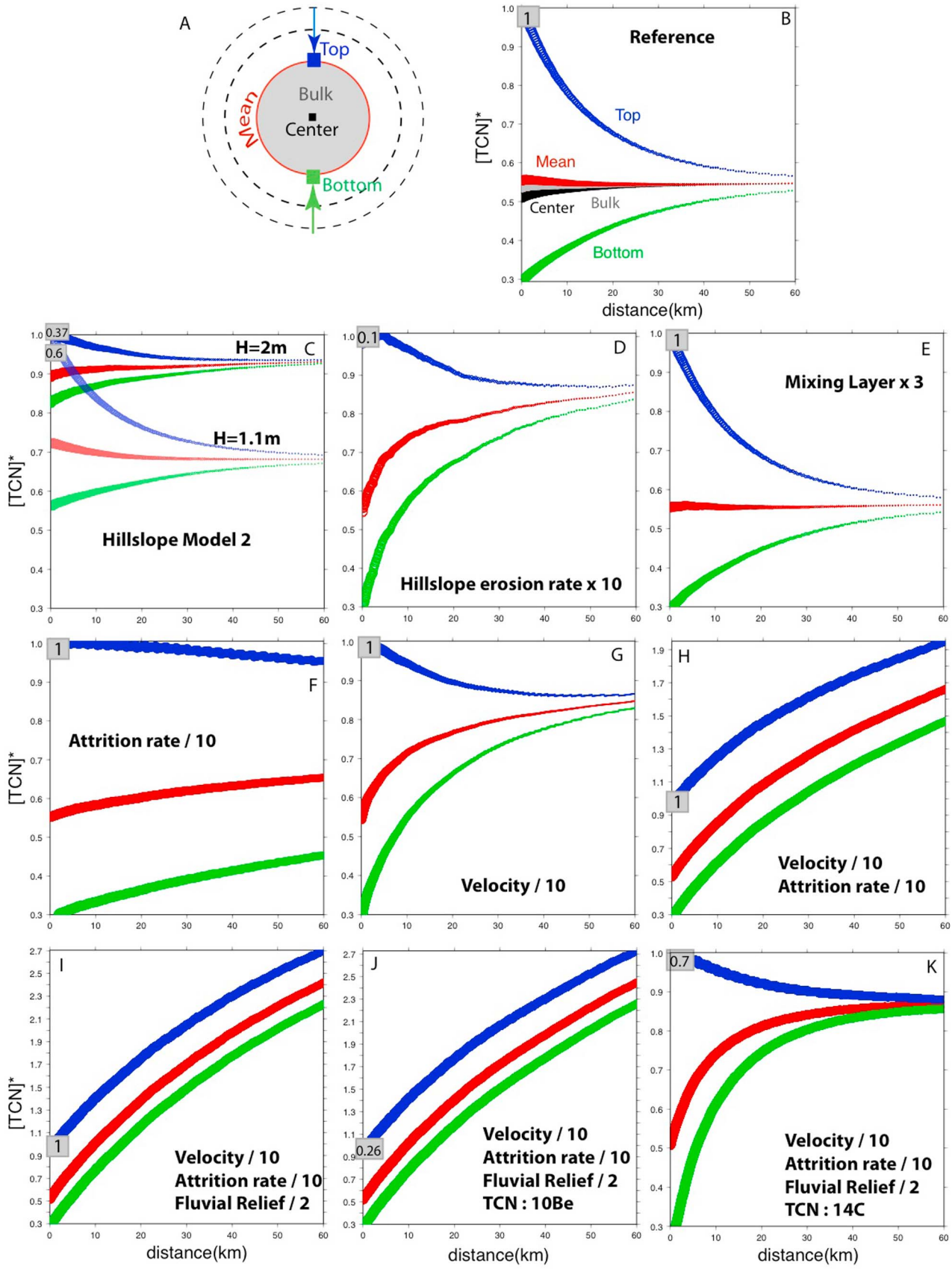
A
Top
Bulk
Center
Mean
Bottom
B
Reference
Top
Mean
Center
Bulk
Bottom
[TCN]*
distance(km)
C
H=2m
H=1.1m
Hillslope Model 2
D
Hillslope erosion rate x 10
E
Mixing Layer x 3
F
Attrition rate / 10
G
Velocity / 10
H
Velocity / 10
Attrition rate / 10
I
Velocity / 10
Attrition rate / 10
Fluvial Relief / 2
J
Velocity / 10
Attrition rate / 10
Fluvial Relief / 2
TCN : 10Be
K
Velocity / 10
Attrition rate / 10
Fluvial Relief / 2
TCN : 14C

Figure 4

rapid abrasion of the clast induces a decrease in surface TCN concentration along the "Top" path due to the exhumation of clast layers which have lower TCN concentrations. On the contrary, attrition removes pieces which are more and more concentrated at the "Bottom". The downstream variation of "Top" is larger than "Bottom" because the initial TCN concentration gradient within the clast displays an exponential function decreasing at depth. A smaller initial clast would present smaller downstream variations for these two points, because the initial TCN concentration gradient within the clast would be smaller. "Top" and "Bottom" correspond to the maximum and minimum TCN concentrations at the clast surface, respectively, if the acquisition of TCN in the river is negligible compared to the hillslope. If not, a long residence time in a river or terrace can change the initial TCN polarity at the clast surface.

[43] Furthermore, "Mean," "Center" and "Bulk" show less than 10% difference and a rapid convergence after a couple of kilometers. The average TCN concentration at the clast surface and center are close because the high TCN production rate on the superior hemisphere is almost balanced by the low production rate on the inferior face. The difference between the mean TCN production rate of the clast surface and center are predicted by equations (A5) and (A6). For a boulder 0.5 m in radius, the relative difference is around 10%. The smaller the clast, the smaller this difference.

[44] Finally, note the small difference between all calculated TCN concentrations when the clast radius is smaller than 5 cm (for travel distances longer than 45 km in Figure 4a). This is important for field sampling: boulders must be sampled at their surface, while small pebbles (<5 cm radius) are usually crushed to obtain the bulk TCN concentration. The similarity between surface and bulk TCN concentrations in small pebbles implies that the measured TCN concentration for boulders and small pebbles can be compared without introducing a sampling bias.

4.2. Parametrical Study

[45] In order to evaluate the model parameters leading to a downstream change in TCN concentrations, we conducted a parameter search by modifying one or several parameters of the reference model. The resulting downstream variations of the TCN concentrations for "Top," "Bottom" and "Mean" are compared to the reference model and shown in Figures 4c–4k.

[46] It is important to fix a detection limit for the downstream variation of the TCN concentrations. We define a *significant* or *detectable* TCN concentration variation to be larger than 15%, a maximum for uncertainty on TCN concentration measurements.

4.2.1. Hillslope Model (Figure 4c)

[47] Hillslope model 2 (soil creep) is tested (non-random T_h) with regolith thicknesses H = 1.1 m and H = 2 m. TCN concentrations vary less than in graph B, because the initial gradient within the clast is smaller for two reasons: (1) the clast moves into the regolith and consequently spends time at depth (the TCN production rate is 20 times lower at 2 m depth), and (2) because it rolls, which limits the TCN concentration polarity at clast surface (see equations (8) and (9)). For H = 2 m, downstream variations are less than 10%, and thus undetectable. This shows that the signal related to attrition disappears rapidly when the regolith thickness increases.

4.2.2. Hillslope Erosion Rate ϵ_h (Figure 4d)

[48] Using a 10 times larger ϵ_h, TCN concentrations show a variation in the trend for "Top" and "Mean". Increasing ϵ_h decreases the residence time of the clast and therefore prevents the development of a strong initial TCN concentration gradient within the clast. Moreover, the river contribution in TCN acquisition is relatively increased. Therefore, the "Top" TCN concentrations decreases less downstream than in the reference model while the "Bottom" concentration increases more downstream. Secondary variations in TCN concentration are due to the stochastic transport in river.

4.2.3. Mixing Layer Thickness, z_{max} (Figure 4e)

[49] Tripling z_{max} does not change the TCN evolution compared to the reference model. A clast spends statistically more time in the fluvial system if z_{max} is larger. However, statistically it resides also at a greater depth. These phenomena balance each other. Nevertheless, increasing z_{max} decreases the mean transport velocity $\overline{V}$ (equation (11)). Therefore, z_{max} needs to be estimated in the field in order to quantify $\overline{V}$ accurately from TCN concentrations [*Nichols et al.*, 2002].

4.2.4. Attrition Rate k (Figure 4f)

[50] A ten-fold decrease of k reduces strongly the decrease of TCN concentration at "Top" and the convergence between curves. The TCN concentrations vary less than 15% downstream and thus become undetectable. Small attrition limits the exhumation of layers with lower TCN concentration. Furthermore, the clast stays longer in the river because the transport velocity is inversely related to clast size (equation (10)). Both processes favor the stability or increase of TCN concentrations within clasts. More generally, decreasing k limits downstream variations due to the initial TCN concentration gradient on hillslopes and favors river TCN acquisition. The strong effect of k on TCN concentration evolution suggests a method to document and quantify attrition. It consists of measuring the TCN concentration of clasts sampled downstream. If attrition is strong, the variance of the TCN concentrations should decrease downstream, the maximum TCN

Figure 4. Downstream evolution of TCN concentrations for a single 0.5 m radius clast for different scenarios. (a) Schematic diagram of the different points, surface or volume of a clast for which (b–k) the TCN concentration is illustrated. In these graphs, the blue curve ("Top") shows the TCN concentration at the top of the clast in its initial position on the hillslope during exhumation (this is not necessarily the TCN concentration at clast top in the river because the clast rolls), the green curve ("Bottom") indicates the opposite point, the red curve ("Mean") is the mean clast surface TCN concentration, the black curve applies to the clast center and the grey curve corresponds to the bulk TCN concentration. The curve thickness is proportional to clast radius. The vertical axis is the TCN concentration normalized by the TCN concentration at "Top" at x = 0 m, the point of entry in the river. ^{21}Ne, ^{10}Be or ^{14}C concentrations used for the normalization are indicated in the upper left corner of corresponding graphs and are expressed in units of 10^6 at/g. Parameters of the reference model (Figure 4b) are given in the text and in Table 1. All graphs but Figure 4c use the hillslope model 1 (shallow landslide) with H = 1 m.

concentration should decrease and the minimum TCN concentration should increase. The difference with the reference model suggests that it could be possible to estimate an order of magnitude of minimum attrition rate k using TCN concentration data from pebbles of a selected lithology.

4.2.5. Clast Velocity β (Figure 4g)

[51] A ten-fold decrease in the velocity gives similar results to an increase in ϵ_h. The clast spends more time in the river, inducing TCN production to balance (exceed) the TCN loss at "Top" ("Mean") due to attrition.

4.2.6. Clast Velocity and Attrition Rate (Figure 4h)

[52] Adding a ten-fold decrease of the velocity and attrition rate leads to a significant increase of all TCN concentrations. In this case, the time spent in the river and the low clast erosion favor TCN acquisition during river transport. The strong difference compared to the original model of graph B suggests that data showing TCN concentration variations may provide an estimate of bounds for β and k.

4.2.7. Clast Velocity, Attrition Rate and Fluvial Relief (Figure 4i)

[53] Decreasing the fluvial relief enhances the increase of TCN concentration observed in the previous case (note different vertical scales in Figures 4h, 4i, and 4j). During its transport in the river, clast elevation decreases, and therefore so does the TCN production rate. Reducing the fluvial relief limits this phenomenon and enhances in-river TCN acquisition.

4.2.8. Clast Velocity, Attrition Rate, Fluvial Relief, and Radioactive Decay (Figures 4j and 4k)

[54] It might be thought that a long in-river period would yield different results for radioactive TCNs. However, Figure 4 shows that the results are similar when we substitute ^{10}Be for ^{21}Ne. ^{10}Be has a decay rate of $\lambda = 4.6 \times 10^{-7}$ a^{-1} and a production rate at sea level ca. 4 times smaller than ^{21}Ne (5.1 at/g/a at high latitude and sea level). The absolute value of the TCN production rate is unimportant when looking at the downstream variation in TCN concentration. Moreover, the decay rate is too small to modify the results significantly in this particular example. Indeed, the residence time of about ~10500 a in the catchment is much lower than the decay time of $1/\lambda$~2 Ma. On the contrary, the "Top" TCN concentration decreases for ^{14}C with a half-life of 5730 a (Figure 4k)."Top" contains the highest hillslope inheritance. Once in the river, this point is buried and loses inherited ^{14}C concentration by radioactive decay. On the contrary, "Bottom" and "Center" accumulate much less ^{14}C on the hillslope because they are deeper. Therefore, they are much more sensitive to ^{14}C production during river transport and thus, their TCN concentrations increase.

4.3. Results for a Population of Clasts

[55] Results for one clast suggest that: (1) if big clasts are sampled along a river, a downstream decrease in maximum and variance of TCN concentrations can highlight a significant attrition rate; (2) an increase of any TCN concentration in a class of clast size allows the river transport rate to be estimated. This section aims to test those ideas on a population of clasts that have different hillslope and in-river histories.

4.3.1. Attrition

[56] A set of experiments has been designed to test the impact on clast TCN concentrations of different sources of variation in hillslope transport. Three experiments are based on the reference model (section 4.1), with different sources of variation (Figure 5): Gaussian variations of T_h (only the biggest clasts are sampled) (Figure 5a), Gaussian variations of T_h and variation in attrition rate k between 1 and 10%/km (only the biggest clasts are sampled) (Figure 5b), Gaussian variations of T_h and different initial clast sizes ([0.1–0.5] m radius) (Figure 5c), and Gaussian variations of T_h, different initial clast sizes ([0.1–0.5] m radius) and a lithological source that extends 500 m horizontally and 500 m vertically on the hillslope (Figure 5d).

[57] Figure 5 shows the downstream evolution of "Top" and "Bottom" for 100 clasts. TCN concentrations are presented as box-and-whisker plots for different downstream distances (Figure 5a). The colored box contains half of the population. The distributions of "Top" and "Bottom" concentrations provide a maximum and minimum for TCN concentrations when the clast surface is sampled randomly.

[58] Figure 5a shows the results for Gaussian variations of T_h on a population of clasts (0.5 m radius), all coming from a specific site at the middle of the hillslope. TCN concentrations on the hillslope (x = 1 km) vary by a factor of 8. The variance and maximum of TCN concentrations decrease downstream (symbolized by the grey lines on Figure 5a), as observed for a single clast (Figure 4b).

[59] We modified the previous experiment to allow the attrition rate k to vary from one clast to another. Figure 5b shows similar features to the previous graph, with a relatively small increase in variance. This suggests that for a weak lithology (large k on average), the clast-to-clast variability in k is not a significant problem, and a mean k can be estimated.

[60] When different clast sizes are taken into account (only clasts bigger than 2.5 cm radius are considered in the populations), scatter grows significantly (Figure 5b). The increase in scatter can be explained by (1) small clasts occupying deeper positions in the landslide layer and (2) differences in the initial TCN concentration gradient within clasts of various sizes.

[61] In the model illustrated by Figure 5d, clasts of different sizes are produced all along the hillslope, simulating an extended lithological source. This modification increases the range of initial TCN production rates (depending on elevation) and clast residence times on the hillslope. Nevertheless, the impact of this modification is minor because most of the variance is already incorporated into the variations related to different initial clast sizes.

[62] These experiments indicate that despite the scatter associated with stochastic processes on a hillslope, the attrition signal can be preserved. In particular, the downstream variations in TCN concentrations (minimum, maximum and variance) are greater than the adopted detection limit of 15%. Scatter can be limited by sampling only the largest clasts.

4.3.2. Sediment Transport Rate

[63] Next, we evaluate if the downstream TCN concentration increase due to river transport is preserved when a population of clasts is considered. The model of Figure 4h, where a significant downstream increase of TCN concentration is expected, is used as reference. Different possible sources of scatter are added (Figure 6): different initial clast sizes ([0.05–0.5] m), Gaussian variations of T_h, and an extended lithological source (500 m high, 500 m long).

[64] Two hillslope models are tested, and the results are shown for two distinct sampling strategies: (1) the whole clast surface ("Mean"), or (2) only a piece of each clast (result between "Bottom" and "Top"). Note that the maximum TCN concentration could be larger than the "Top" one because

some clasts can be trapped for a long time in-river, accumulating TCN in a way that modifies the initial clast polarity acquired on the hillslope. Numerical modeling of the true TCN maximum would require the discretization of the clasts into numerous elements, which is beyond the scope of the present study.

[65] Results show similar trends for both models: a significant increase in the average TCN concentration, but different scatter. In sampling strategy 1 ("Mean" in Figures 6a and 6c), scatter is smaller because the calculated TCN concentration is an average of the different points on the clast surface. When randomly sampling a part of each clast (strategy 2), the scatter expected for model 1 (shallow landslides) is larger than for model 2 (regolith) (Figures 6b and 6d). Indeed, during the clast movement in the hillslope regolith, the clast rolls and its surface concentration tends to homogenize. This process limits the clast-to-clast variation.

[66] Finally, the variance of TCN concentrations increases downstream mainly because small clasts travel faster than big clasts, and secondly because clasts have different paths in the mixing layer. Limiting the sampling to a specified clast size reduces the scatter and may allow us to evaluate if transport velocity depends on clast size (Figure 7).

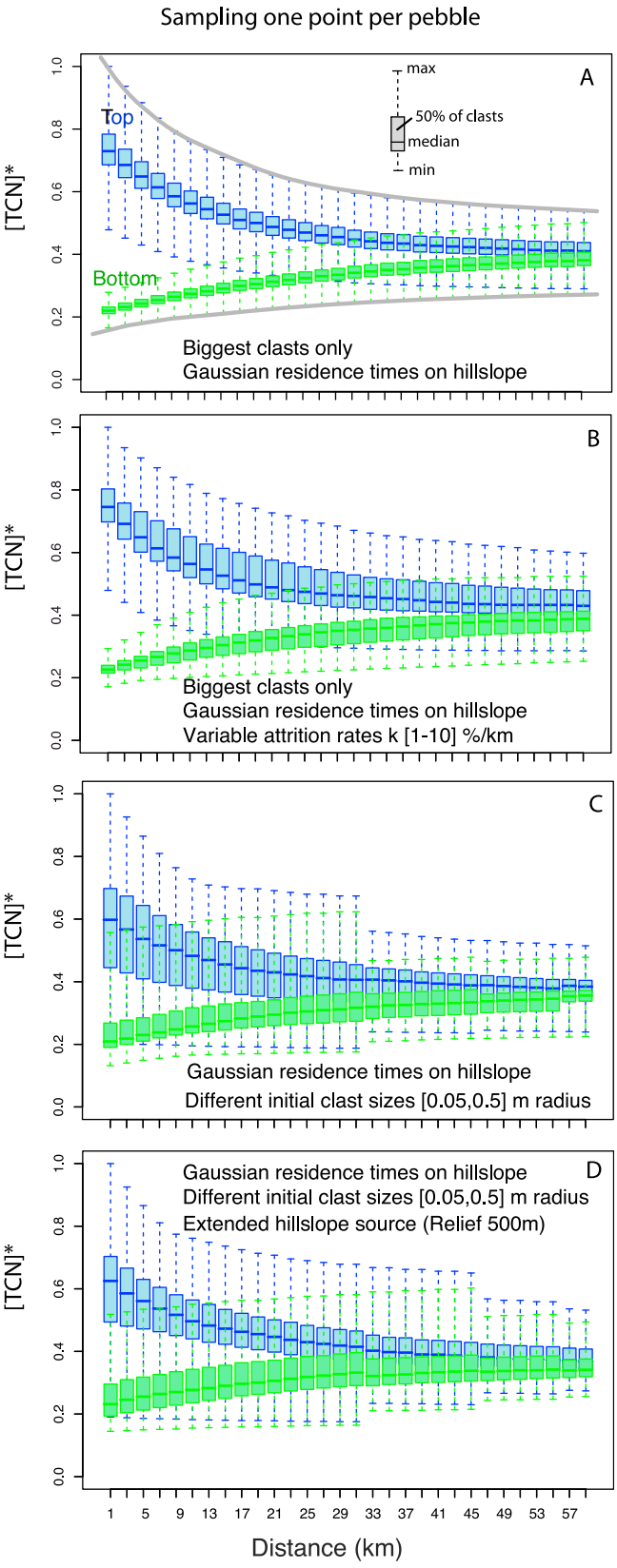

Figure 5. (a–d) Model results for a population of clasts (100) using model parameters for which the attrition signal dominates. Parameters are those of the reference model (Figure 4b and Table 1). Box-and-whisker plots correspond to TCN concentrations at diametrically opposite points along the vertical axis during exhumation on the hillslope ("Top" and "Bottom"). The grey lines in Figure 5a symbolize the range of expected TCN concentrations if clasts are sampled randomly by taking a sample at clast surface for boulders, or the whole clast for pebbles. Figures 5a–5d correspond to different sources of variability, as indicated on the graphs. Gaussian variations of T_h have a standard deviation of $T_h/4$. On the vertical axis, ^{21}Ne concentrations are normalized by the maximum ^{21}Ne concentration: 1.5×10^6 at/g (Figure 5a), 1.45×10^6 at/g (Figure 5b), 1.26×10^6 at/g (Figure 5c), and 1.34×10^6 at/g (Figure 5d). The sudden decrease in the size of the whiskers in Figures 5c and 5d at some stage downstream are due to the selection of clasts larger than 2.5 cm in radius, which removes outliers.

5. Discussion

[67] Our results reveal that the attrition rate k and the long-term mean velocity $\overline{V}$ (equation (11)) can be bracketed using TCN concentration data in two cases: (1) There is a significant downstream increase (>15%) of the mean TCN concentration in pebbles (leading to $\overline{V}$), or (2) There is a significant downstream decrease (>15%) in the clast-to-clast variance and maximum of TCN concentration variance (leading to k). The limitation of such scenarios could be the natural variability of erosion processes. Some of these processes have been incorporated in the model, but others are discussed in the following section.

5.1. Other Potential Sources of Scatter

[68] The model excludes shielding related to the topographic gradient on the hillslope, which can modify the TCN concentration distribution within boulders [*Lal and Chen*, 2005]. However, the gradient effect would not prevent the existence of TCN concentration polarity on the hillslope. Consequently, the slope effect does not modify the prediction of a downstream convergence of TCN con-

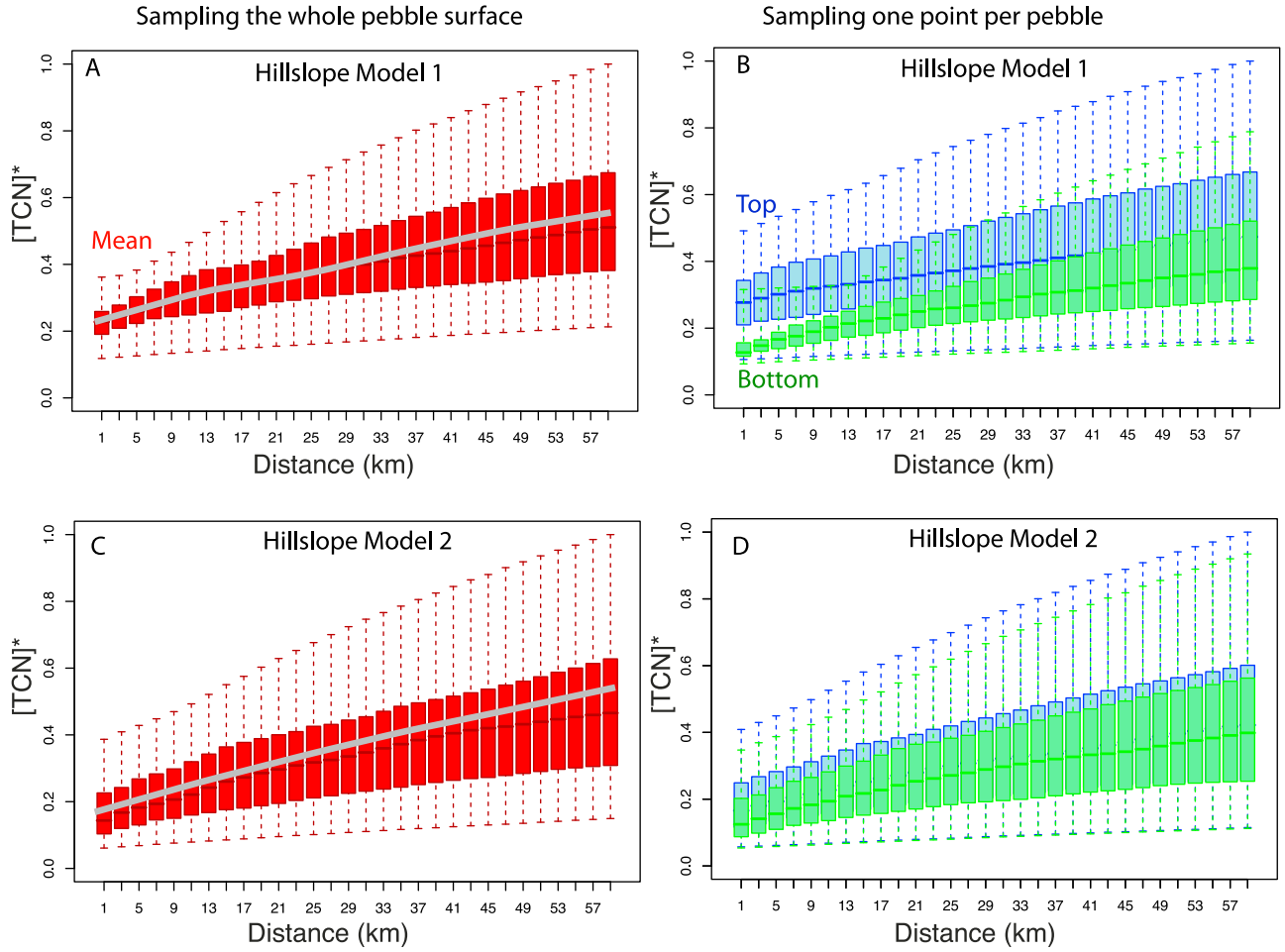

Figure 6. (a–d) Model results for a population of clasts in the case of parameters that favor a downstream increase in TCN ^{21}Ne concentration. Parameters for Figures 6a and 6b correspond to those of Figure 4i. Compared to the reference model, the relief is divided by 2, the velocity is divided by 10, and the attrition rate is divided by 10. The sources of variability include different initial locations on the hillslope (500 m long and 500 m high), Gaussian variations of T_h, variable clast sizes in the range [0.05–0.5] m radius and stochastic transport in the river. Figures 6c and 6d use the same parameters but with hillslope model 2 (H = 1.1 m). In Figures 6a and 6c, the grey line corresponds to the mean TCN concentration of the clast population. On the vertical axis, ^{21}Ne concentrations are normalized by the maximum ^{21}Ne concentration: 2.6×10^6 at/g (Figure 6a), $3. \times 10^6$ at/g (Figure 6b), 2.9×10^6 at/g (Figure 6c), and $3. \times 10^6$ at/g (Figure 6d).

centrations. For a significant TCN acquisition during river transport, the hillslope gradient effect is negligible. Furthermore, the model assumes that a clast is always buried below the Earth's surface. Therefore, allowing the clast to be partly exposed would affect the TCN concentration distribution within the clast [*Lal and Chen*, 2005]. For example, the average TCN concentration at the clast surface and the surface-to-center gradient would be greater. In this case and for strong attrition, the downstream decrease of TCN concentration differences within a clast could be greater than predicted by the model.

[69] The model assumes spherical clasts. Clasts can have variable shapes in nature, especially at the catchment head. Shape differences may increase the expected TCN concentration variance. The mean surface production rate can be calculated for a parallelepiped and compared to a sphere (Appendix B). The relative difference is lower than 20% between a 1 m sphere and a parallelepiped with shape ratio of 2 (Appendix B). The difference between "Top" and "Bottom" should be the same if the clast is buried and if the density difference between the considered clast and the surrounding material is not too large. In these cases, the TCN production rates at these two points do not depend on the shape of the considered clast but only on their depth. Consequently, it is not likely that a shape difference would significantly increase the scatter already incorporated in the model (variations in residence depth, size, location and time on hillslope). Clast shape should not be a problem when river transport increases TCN concentrations from a variety of sources.

[70] Our hillslope models assume a homogeneous regolith or landslide depth over the hillslope. If H varies downhill in the range of several meters, clasts can develop variable TCN concentration gradients depending on where they were exhumed. This would have the same qualitative effect as increasing H in the hillslope models, namely, increasing the

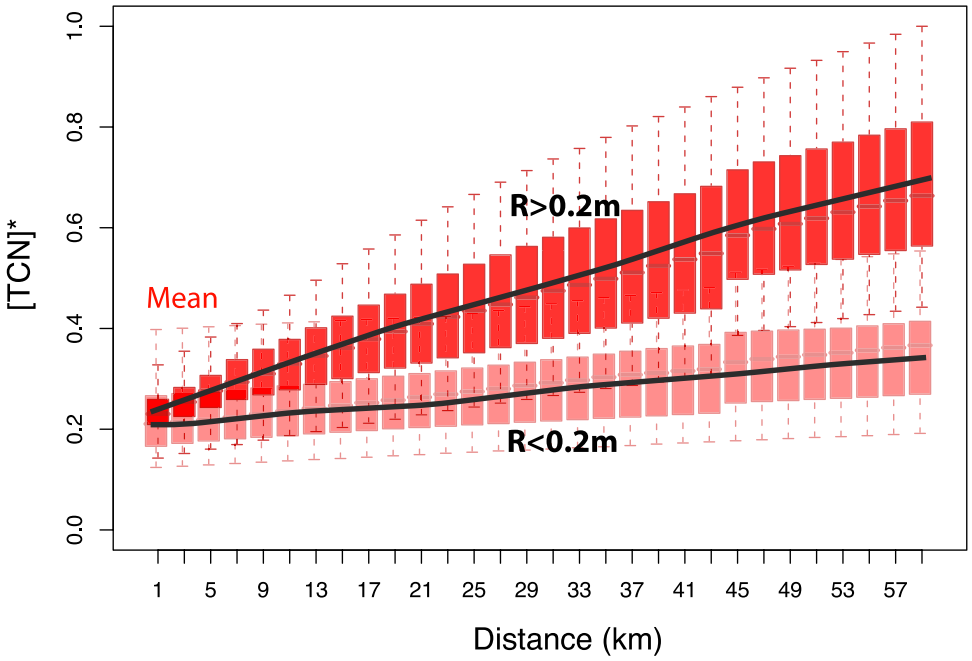

Figure 7. Same as Figure 6a, but with clasts separated into two populations: clast radius <0.2 m and >0.2 m. Black lines illustrate the population averages. The different evolutions are explained by the different velocities for small and big clasts.

clast-to-clast scatter. Part of this scatter may already be incorporated in the Gaussian variations imposed on residence times on the hillslope.

[71] In hillslope model 2, the TCN concentration does not integrate the decrease in production rate as the clast travels downhill. This simplification overestimates TCN concentrations. This overestimation is larger for clasts coming from higher elevations. A better model would reduce the calculated difference of TCN concentrations between clasts exhumed at different locations on the hillslope (less scatter).

[72] Significant erosion of a boulder has been simplified by considering erosion only when the clast moves. Large boulders can roll, as cited in *Turowski et al.* [2009], or observed by us in Patagonian rivers. However, boulders can be also eroded by other clasts while they are embedded in the riverbed or by weathering within terraces. The relative efficiency of these processes is poorly known. If the top of a fixed boulder erodes very rapidly, the difference in TCN concentrations between its top and bottom will decrease. So, in situ erosion should yield a similar trend as that predicted with our simplified model of clast attrition, but it remains to be tested.

[73] The shielding effect of water during transport has not been taken into account. It can prevent significant in-river TCN acquisition by reducing the TCN production rate at the clast surface. Attenuation in water is 2.7 times lower than in granite, so approximately 12 m of water is necessary to almost cancel TCN production by spallation. This can easily be added into the model for a specific field case, for example by reducing the production rate at the Earth's surface in the river.

[74] The effect of landslides has been studied by assuming a uniform probability distribution for clast depths and a Gaussian distribution for residence times. If the clast depth actually followed a power law function (shallow clasts more numerous than deep ones), then more clasts would reside closer to the surface. The proportion of clasts with large TCN concentration values would increase. In Figures 5 and 6, the distributions of TCN concentrations at each river station would be much less symmetrical, with means shifted toward larger values. The precise effect of different frequency distributions of landslides and clast sizes should be tested in the future, in particular to evaluate if the distribution of TCN concentrations of a clast population can provide quantitative information about the frequency distribution of landslides. Similarly, the river transport model could be improved by incorporating specific "non-local" transport rules leading to power law distributions of clast hop lengths that have been evidenced recently [e.g., *Bradley et al.*, 2010; *Foufoula-Georgiou et al.*, 2010; *Ganti et al.*, 2011; *Hill et al.*, 2010; *Stark et al.*, 2009; *Tucker and Bradley*, 2010].

5.2. Is a TCN Concentration Increase or Decrease Downstream Realistic?

[75] A fundamental question remains: can other processes produce a downstream TCN concentration decrease that could be misinterpreted as a consequence of clast abrasion? Two different processes can produce this effect: radioactive decay and a selective downstream sorting based on clast size. However, the first process is unlikely to play a significant role, except for very short-lived TCNs (e.g., Figure 4k). The second process can be very efficient if sedimentation occurs. Selective deposition can lead to a downstream fining of the sediment mixture [*Paola et al.*, 1992a]. This process could produce a downstream decrease of TCN concentration variance that does not reflect clast abrasion but rather differences in the initial (hillslope) TCN concentration between small and large clasts. *Attal and Lavé* [2006] suggested that experimentally derived abrasion coefficients can account for the

downstream evolution of pebbles without calling for additional fining processes, in particular near the channel head where clast abrasion can be large. Moreover, the existence of a TCN concentration-clast size relationship can be verified near the sediment production source. If it is not present, or is inverted (cobbles have lower TCN concentration than sand [cf. *Belmont et al.*, 2007]), clast abrasion is necessary to decrease the "Top" TCN concentration downstream. Therefore our proposed method could provide a way to quantify k even in the case of downstream fining due to selective deposition.

[76] Our results suggest that $\overline{V}$ can be easily quantified if the TCN concentration increases downstream. However, is a TCN concentration increase likely? As discussed by *Carretier et al.* [2009b], this depends mainly on the sediment budget in the catchment, i.e., whether the catchment is eroding or accumulating sediment, and on the mixing layer thickness. Theoretically, a significant TCN concentration increase can be found in even small catchments experiencing sedimentation because in-river clast residence times can be relatively long compared to hillslope residence times [*Carretier et al.*, 2009b]. A thick mixing layer and water depth (although not taken into account in this model) can strongly limit TCN concentration acquisition in rivers. For example, *Wittmann et al.* [2009] obtained a constant TCN concentration in sand along the Amazon River. The depth of the water and the probably thick mixing layer may have prevented a significant increase in TCN concentration. On the contrary, slow transport in the Mojave desert over a piedmont with a small sedimentation rate and a thin mixing layer led to a significant TCN concentration increase, allowing *Nichols et al.* [2002, 2005] to quantify a sediment (mostly sand) transport rate of about 16 cm/a. Such a rate is consistent with our results, suggesting that a TCN concentration increase in our reference mountain river with a thicker mixing layer requires transport rates of $\overline{V} < 20$ m/a. This is quite small compared to transport lengths obtained from magnetic tracers in pebbles over periods of several years [*Pyrce and Ashmore*, 2003]. Nevertheless, small mean velocities remain possible if they correspond to longer periods that include rest at depth or in terraces. Such low velocities are more probable in piedmont rivers, as shown for example by *Nichols et al.* [2002, 2005]. Additional examples of slow transport rates were provided by *Vigier et al.* [2001], *Dosseto et al.* [2006], *Chabaux et al.* [2006] and *Granet et al.* [2007] who used U series elements to determine mean clast velocities ranging between 1 and 20 m/a for sand in the Amazon and Ganges plains, respectively.

5.3. Sampling Strategy

[77] It is crucial that the sampled lithology has a unique source in the catchment in order to avoid complexities due to mixed sources [*Binnie et al.*, 2006; *Carretier et al.*, 2009b]. As far as the dominant effect (attrition or transport rate) is not known a priori, the following strategies are proposed. We suggest limiting the analysis to the coarsest fraction of the clast population on hillslopes and in the river. Clasts belonging to this fraction are often smaller than 1 m diameter [e.g., *Attal and Lavé*, 2006], which may constitute a maximum size for the sampling. Although this value can vary from place to place, larger boulders are more likely to have a different behavior on hillslopes and in the river. One surface section of different clasts is sampled randomly at different stations along the river, from the lithological source to the outlet. The largest clasts of the grain-size distributions are selected, even if clasts size decreases downstream (significant attrition or selective deposition). Limiting the analysis to the coarsest fraction at each river station should limit the scatter associated with different initial clast sizes. Alternatively, clasts can be grouped by size in order to study size-dependent transport. Each clast is then treated separately to obtain a population of TCN concentrations. Using this set of samples, the downstream evolution of the TCN concentration distributions (max, mean and variance) can be studied.

[78] The study of the downstream evolution of clast-to-clast TCN concentration is quite time-consuming and expensive. 150 samples for one river (5 sites × 30 clasts) seems to be the minimum to study how the scatter of TCN concentrations evolves downstream. Consequently, it is necessary to make first-order observations to evaluate the potential for studying the clast-to-clast TCN concentration difference in a field case. If the largest clasts are smaller than 0.15 m radius close to the source, it is probably not possible to observe a TCN concentration evolution associated with attrition because the initial TCN concentration gradient within such small clasts is too small. Moreover, if the dominant erosion process on the hillslope corresponds to deep landslides or a thick regolith ($\gg 2m$), there is little chance that all clasts can develop a significant gradient. In both cases, measuring the TCN concentration for each clast may be useless. Alternatively, a larger number of samples (>30) can be mixed for 10 river stations in order to obtain an average TCN concentration for the population at each station (the grey curve in Figure 6 for example). Even if the sampling corresponds to parts of clasts, their mixing should give an estimate of the mean TCN concentration population (e.g., black lines in Figure 7). These means can be fitted by the model to estimate the mean transport velocity between stations. In any case, this mixing approach should be carried out first and the TCN concentration of individual clasts should be measured in a second step.

[79] Some parameters can be estimated in the field. For example, the mixing layer thickness z_{max} may correspond to a typical bar height in a braided river, or the bankfull river depth in a meandering river. Scour and fill events can be quantified using scour chains [e.g., *Laronne et al.* 1994]. However, the mixing layer and scour should depend on the timespan under consideration: a longer period includes extreme erosion-deposition events that increase the thickness of the mixing layer. Actually, the mixing layer is a conceptual simplification of a more diffuse and time-variable zone of sediment mixing [*Parker et al.*, 2000]. Nevertheless, a maximum value can probably be estimated. For example, in the Amazon near Iquitos, 10-meter dunes are moving along the river bed, which may correspond to the mixing layer thickness (J. L. Guyot, personal communication, 2008). A mixing depth of approximately 30 cm was identified by *Nichols et al.* [2002] in ephemeral piedmont rivers using TCN concentration depth profiles.

[80] Attrition rate k can be estimated by measuring the proportion of pebbles from selected lithologies in the river provided that the erosion rates of the corresponding source areas are known [*Attal and Lavé*, 2006]. The hillslope erosion rates ϵ_h of selected lithologies may be determined from the TCN concentration of sand sampled at the foot of corresponding areas on hillslopes, although landsliding and

mixing with other sources in the river could potentially yield significant error [e.g., *Granger et al.*, 1996; *Yanites et al.*, 2009]. In addition, if our proposed method can provide k values in a catchment where the distribution of denudation rates is unknown, then we can derive the rate at which units with a given k are eroded by looking at the relative proportion of rock types in the sediment.

6. Conclusion

[81] We propose a model for downstream evolution of TCN concentrations within clasts. This model suggests that bounds on the clast abrasion k and the long-term average clast velocity $\overline{V}$ can be determined from TCN concentration data in some favorable cases. These cases correspond to hillslope processes dominated by shallow landslides and a unique TCN-rich lithology in the catchment, so that clasts of the same lithology from the same source can be gathered along the river course.

[82] The model allows a sampling strategy to be proposed. It consists of sampling a point of the largest clasts (<1 m) at different stations in the river from source to outlet. A downstream decrease in maximum and variance of TCN concentrations indicates and permits quantification of the attrition rate. An increase of the average TCN concentration at each station can be used to quantify the mean transport rate of coarse sediments.

[83] The next step is to measure the TCN concentration of big clasts in rivers with a localized lithological source. In any case, our results should help understand the along-stream evolution of TCN concentration in gravels, pebbles and boulders, a prerequisite to using TCN concentrations at river outlet to quantify erosion rates for specified lithological units in a catchment, and to using TCN concentration in clasts as tracer of erosion processes.

Appendix A: TCN Production Rate for a Spherical Clast Layer

[84] We consider a spherical layer of radius r in a clast of radius R, the top of the clast being at a depth z_s relative to the surface of the Earth (Figure 2). The mean TCN concentration averaged over the layer of radius r is given by:

$$P_r = \int_0^{\pi} P_s e^{-z/\mu} \frac{2\pi r \sin\theta \, r d\theta}{4\pi r^2} \tag{A1}$$

with P_s the production rate at the Earth's surface, calculated using the parameters in *Stone* [2000], μ an attenuation length [L] associated with a particle type, and

$$z = z_s + R - r\cos\theta \tag{A2}$$

so that

$$P_r = 0.5\,\mu\, e^{-z_s/\mu}\, e^{-R/\mu}\, \frac{\left(e^{r/\mu} - e^{-r/\mu}\right)}{r}\, P_s \tag{A3}$$

or

$$P_r = F_r\, e^{-z_s/\mu}\, P_s \tag{A4}$$

with

$$F_r = 0.5\,\mu\, e^{-R/\mu}\, \frac{\left(e^{r/\mu} - e^{-r/\mu}\right)}{r}. \tag{A5}$$

[85] F_r is a scaling factor, such that the mean production rate P_r decreases with a larger R. For a given R, it increases with r. For example, the mean production rate at the surface of a 0.5 m radius clast (the top of which is at the Earth's surface) is half the production rate at the Earth's surface.

[86] Equation (A1) is also the mean TCN production rate at a point on the layer of a continuously rolling clast. Indeed, P_r is the sum of the production rates at varying depths z multiplied by the probability $\frac{2\pi r \sin\theta}{4\pi r^2} r d\theta$ that this point is between depths z and $z + dz$. This equivalence is fundamental because it allows the use of this average TCN concentration whether the boulder has been rolling or not, assuming that boulder is sampled at different points around its surface.

[87] Note that for the clast center

$$F_0 = e^{-R/\mu} \tag{A6}$$

The total production rate for neutrons, fast muons and stop muons is obtained by

$$P_r = \sum_{I=1,3} \chi_i F_{ri}\, e^{-z_s/\mu_i}\, P_s \tag{A7}$$

where the subscript i refers to each particle type and χ_i is their respective contribution [*Braucher et al.*, 2003] (see Table 1).

Appendix B: TCN Production Rate at the Surface of a Parallelepiped

[88] In order to compare the effect of clast shape on its mean surface TCN concentration, the mean surface TCN production rate is calculated for a parallelepiped of sides a, b and c, assuming that the block rolls and its top is at depth z_s. The mean TCN production rate is

$$P_p = F_p\, e^{-z_s/\mu}\, P_s \tag{B1}$$

where the scaling factor is

$$F_p = \frac{2}{3}\left(b\mu\left(1 - e^{-c/\mu}\right) + a\mu\left(1 - e^{-c/\mu}\right)\right) \tag{B2}$$

$$+\frac{2}{3}\left(c\mu\left(1 - e^{-b/\mu}\right) + a\mu\left(1 - e^{-b/\mu}\right)\right) \tag{B3}$$

$$+\frac{2}{3}\left(b\mu\left(1 - e^{-a/\mu}\right) + c\mu\left(1 - e^{-a/\mu}\right)\right) \tag{B4}$$

$$+\frac{1}{3}\, ab\left(1 + e^{-c/\mu}\right) \tag{B5}$$

$$+\frac{1}{3}\, ac\left(1 + e^{-b/\mu}\right) \tag{B6}$$

$$+\frac{1}{3}\, bc\left(1 + e^{-a/\mu}\right). \tag{B7}$$

[89] For a cube of 1 m^3, F_p is 0.52, that is 6% larger than F_r calculated for a sphere of 1m diameter. If one considers a

parallelepiped of size 1 m × 0.75 m × 0.5 m, F_p is 22% larger than F_r calculated for a sphere of 1 m diameter. This percentage decreases when the cube and sphere size decrease.

[90] **Acknowledgments.** This study was funded by the IRD, the French national research agency ANR (project "ANDES" ANR-06-JCJC-0100), and the Institut des Sciences de l'Univers, CNRS, project SESPEED. S. Carretier thanks the Department of Geology of the University of Chile for its warm welcome. We thank Stephanie Brichau and Judit Orsay for English editing. We thank E. Pepin and J. Martinod for constructive comments on a previous manuscript, B. J. Yanites, S. Brocklehurst (Associate Editor), M. Attal, and an anonymous reviewer for outstanding reviews that helped us improve this paper.

References

Allen, P. (2008), Time scales of tectonic landscapes and their sediment routing systems, in *Landscape Evolution: Denudation, Climate and Tectonics over Different Time and Space Scales*, edited by K. Gallagher, S. J. Jones, and J. Wainwright, *Geol. Soc. Spec. Publ.*, *296*, 7–28.

Attal, M., and J. Lavé (2006), Changes of bedload characteristics along the Marsyandi River (central Nepal): Implications for understanding hillslope sediment supply, sediment load evolution along fluvial networks, and denudation in active orogenic belts, in *Tectonics, Climate, and Landscape Evolution*, edited by S. Willett et al., *Spec. Pap. Geol. Soc. Am.*, *398*, 143–171, doi:10.1130/2006.2398(09).

Attal, M., and J. Lavé (2009), Pebble abrasion during fluvial transport: Experimental results and implications for the evolution of the sediment load along rivers, *J. Geophys. Res.*, *114*, F04023, doi:10.1029/2009JF001328.

Belmont, P., F. Pazzaglia, and J. Gosseb (2007), Cosmogenic ^{10}Be as a tracer for hillslope and channel sediment dynamics in the Clearwater River, western Washington State, *Earth Planet. Sci. Lett.*, *264*, 123–135, doi:10.1016/j.epsl.2007.09.013.

Binnie, S., W. Phillips, M. Summerfield, and L. Fifield (2006), Sediment mixing and basin-wide cosmogenic nuclide analysis in rapidly eroding mountainous environments, *Quat. Geochronol.*, *1*, 4–14, doi:10.1016/j.quageo.2006.06.013.

Bradley, D., G. Tucker, and D. Benson (2010), Fractional dispersion in a sand bed river, *J. Geophys. Res.*, *115*, F00A09, doi:10.1029/2009JF001268.

Braucher, R., E. Brown, D. Bourles, and F. Colin (2003), In situ produced 10Be measurements at great depths: implications for production rates by fast muons, *Earth Planet. Sci. Lett.*, *211*, 251–258, doi:10.1016/S0012-821X(03)00205-X.

Brewer, P., and J. Lewin (1993), In-transport modification of alluvial sediment: Field evidence and laboratory experiments, in *Alluvial Sedimentation*, edited by M. Marzo and C. Puigdefabregas, *Spec. Publ. Int. Assoc. Sedimentol.*, *17*, 23–35.

Carretier, S., and F. Lucazeau (2005), How does alluvial sedimentation at range fronts modify the erosional dynamics of mountain catchments?, *Basin Res.*, *17*, 361–381, doi:10.1111/j.1365-2117.2005.00270.x.

Carretier, S., B. Poisson, R. Vassallo, E. Pepin, and M. Farias (2009a), Tectonic interpretation of transient stage erosion rates at different spatial scales in an uplifting block, *J. Geophys. Res.*, *114*, F02003, doi:10.1029/2008JF001080.

Carretier, S., V. Regard, and C. Soual (2009b), Theoretical cosmogenic nuclide concentration in river bedload clasts: Does it depend on clast size?, *Quat. Geochronol.*, *4*, 108–123, doi:10.1016/j.quageo.2008.11.004.

Castelltort, S., and J. van den Driessche (2003), How plausible are high-frequency sediment supply-driven cycles in the stratigraphic record?, *Sediment. Geol.*, *157*, 3–13, doi:10.1016/S0037-0738(03)00066-6.

Chabaux, F., M. Granet, E. Pelt, C. France-Lanord, and V. Galy (2006), ^{238}U-^{234}U-^{230}Th disequilibria and timescale of sedimentary transfers in rivers: clues from the Gangetic plain rivers, *J. Geochem. Explor.*, *88*, 373–375.

Charru, F. (2006), Selection of the ripple length on a granular bed sheared by a liquid flow, *Phys. Fluids*, *18*, 121508, doi:10.1063/1.2397005.

Chatanantavet, P., E. Lajeunesse, G. Parker, L. Malverti, and P. Meunier (2010), Physically based model of downstream fining in bedrock streams with lateral input, *Water Resour. Res.*, *46*, W02518, doi:10.1029/2008WR007208.

Church, M. (2006), Bed material transport and the morphology of alluvial river channels, *Annu. Rev. Earth Planet. Sci.*, *34*, 325–354, doi:10.1146/annurev.earth.33.092203.122721.

Church, M., and M. Hassan (1992), Size and distance of travel of unconstrained clasts on a streambed, *Water Resour. Res.*, *28*, 299–303, doi:10.1029/91WR02523.

Codilean, A. T., P. Bishop, T. B. Hoey, F. M. Stuart, and D. Fabel (2010), Cosmogenic Ne-21 analysis of individual detrital grains: Opportunities and limitations, *Earth Surf. Processes Landforms*, *35*, 16–27, doi:10.1002/esp.1815.

Cowie, P. A., A. Whittaker, M. Attal, G. Roberts, G. E. Tucker, and A. Ganas (2008), New constraints on sediment-flux-dependent river incision: Implications for extracting tectonic signals from river profiles, *Geology*, *36*, 535–538, doi:10.1130/G24681A.1.

Crosby, B., K. Whipple, N. Gasparini, and C. Wobus (2007), Formation of fluvial hanging valleys: Theory and simulation, *J. Geophys. Res.*, *112*, F03S10, doi:10.1029/2006JF000566.

Davy, P., and D. Lague (2009), Fluvial erosion/transport equation of landscape evolution models revisited, *J. Geophys. Res.*, *114*, F03007, doi:10.1029/2008JF001146.

Dosseto, A., B. Bourdon, J. Gaillardet, L. Maurice-Bourgoin, and C. Allegre (2006), Weathering and transport of sediments in the Bolivian Andes: Time constraints from uranium-series isotopes, *Earth Planet. Sci. Lett.*, *248*, 759–771.

Farias, M., Charrier, D. Comte, J. Martinod, and G. Herail (2005), Late Cenozoic deformation and uplift of the western flank of the Altiplano: Evidence from the depositional, tectonic, and geomorphologic evolution and shallow seismic activity (northern Chile at 19° 30′S), *Tectonics*, *24*, TC4001, doi:10.1029/2004TC001667.

Ferguson, R., and S. Wathen (1998), Tracer-pebble movement along a concave river profile: Virtual velocity in relation to grain size and shear stress, *Water Resour. Res.*, *34*, 2031–2038.

Ferguson, R., T. Hoey, S. Wathen, and A. Werritty (1996), Field evidence for rapid downstream fining of river gravel through selective transport, *Geology*, *24*, 179–182.

Foufoula-Georgiou, E., V. Ganti, and W. Dietrich (2010), A nonlocal theory of sediment transport on hillslopes, *J. Geophys. Res.*, *115*, F00A16, doi:10.1029/2009JF001280.

Ganti, V., K. M. Straub, E. Foufoula-Georgiou, and C. Paola (2011), Space-time dynamics of depositional systems: Experimental evidence and theoretical modeling of heavy-tailed statistics, *J. Geophys. Res.*, *116*, F02011, doi:10.1029/2010JF001893.

Gasparini, N. M., R. L. Bras, and K. Whipple (2006), Numerical modeling of non-steady-state river profile evolution using a sediment-flux-dependent incision model, in *Tectonics, Climate, and Landscape Evolution*, edited by S. Willet et al., *Spec. Pap. Geol. Socl. Am.*, *398*, 127–141, doi:10.1130/2006.2398(08).

Gosse, J., and F. Phillips (2001), Terrestrial in situ cosmogenic nuclides: theory and application, *Quat. Sci. Rev.*, *20*, 1475–1560.

Granet, M., F. Chabaux, P. Stille, C. France-Lanord, and E. Pelt (2007), Time-scales of sedimentary transfer and weathering processes from U-series nuclides: Clues from the Himalayan rivers, *Earth Planet. Sci. Lett.*, *261*, 389–406, doi:10.1016/j.epsl.2007.07.012.

Granger, D., J. Kircher, and R. Finkel (1996), Spatially averaged long-term erosion rates measured from in situ-produced cosmogenic nuclides in alluvial sediment, *J. Geol.*, *104*, 249–257.

Guzzetti, F., B. Malamud, D. Turcotte, and P. Reichenbach (2002), Power-law correlations of landslide areas in central Italy, *Earth Surf. Processes Landforms*, *195*, 169–183.

Guzzetti, F., M. Galli, P. Reichenbach, F. Ardizzone, and M. Cardinali (2006), Landslide hazard assessment in the Collazzone area, Umbria, Central Italy, *Nat. Hazards Earth Syst. Sci.*, *6*, 115–131.

Heimsath, A., J. Chappell, N. Spooner, and D. Questiaux (2002), Creeping soil, *Geology*, *30*, 111–114.

Hill, K., L. DellAngelo, and M. Meerschaert (2010), Heavy-tailed travel distance in gravel bed transport: An exploratory enquiry, *J. Geophys. Res.*, *115*, F00A14, doi:10.1029/2009JF001276.

Hovius, N., C. P. Stark, and P. A. Allen (1997), Sediment flux from a mountain belt derived by landslide mapping, *Geology*, *25*, 231–234.

Hovius, N., C. P. Stark, C. Hao-Tsu, and L. Jiun-Chuan (2000), Supply and removal of sediment in a landslide-dominated mountain belt: Central Range, Taiwan, *J. Geol.*, *108*, 73–89.

Jones, L. S., and N. F. Humphrey (1997), Weathering-controlled abrasion in a coarse-grained, meandering reach of the Rio Grande: Implications for the rock record, *Geol. Soc. Am. Bull.*, *109*, 1080–1088, doi:10.1130/0016-7606(1997)109<1080:WCAIAC>2.3.CO;2.

Kirchner, J. W., R. Finkel, C. Riebe, D. Granger, J. Clayton, J. King, and W. Megahan (2001), Mountain erosion over 10-year, 10,000-year, and 10,000,000-year timescales, *Geology*, *29*, 591–594.

Knighton, A. (1982), Longitudinal changes in the size and shape of stream bed material: Evidence of variable transport conditions, *Catena*, *9*, 23–34.

Lague, D. (2010), Reduction of long-term bedrock incision efficiency by short-term alluvial cover intermittency, *J. Geophys. Res.*, *115*, F02011, doi:10.1029/2008JF001210.

Lal, D., and J. Chen (2005), Cosmic ray labeling of erosion surfaces II: Special cases of exposure histories of boulders, soils and beach terraces, *Earth Planet. Sci. Lett.*, *236*, 797–813, doi:10.1016/j.epsl.2005.05.025.

Laronne, J., D. Outhet, P. Carling, and T. McCabe (1994), Scour chain employment in gravel-bed rivers, *Catena*, *22*, 299–306.

Larsen, I. J., D. R. Montgomery, and O. Korup (2010), Landslide erosion controlled by hillslope material, *Nat. Geosci.*, *3*, 247–251, doi:10.1038/NGEO776.

Liu, Y., F. Metivier, E. Lajeunesse, P. Lancien, and P. Meunier (2008), Measuring bed load in gravel-bed mountain rivers: Averaging methods and sampling strategies, *Geodin. Acta*, *21*, 81–82.

Malmaeus, J., and M. Hassan (2002), Simulation of individual particule movement in a gravel streambed, *Earth Surf. Processes Landforms*, *27*, 81–97, doi:10.1002/esp.305.

Metivier, F., and Y. Gaudemer (1999), Stability of output fluxes of large rivers in South and East Asia during the last 2 million years: Implications on floodplain processes, *Basin Res.*, *11*, 293–303.

Metivier, F., Y. Gaudemer, P. Tapponnier, and M. Klein (1999), Mass accumulation rates in Asia during the Cenozoic, *Geophys J Int.*, *137*, 280–318, doi:10.1046/j.1365-246X.1999.00802.x.

Nichols, K. K., P. R. Bierman, R. Hooke, E. M. Clapp, and M. W. Caffee (2002), Quantifying sediment transport on desert piedmonts using ^{10}Be and ^{26}Al, *Geomorphology*, *45*, 105–125.

Nichols, K. K., P. R. Bierman, M. W. Caffee, R. Finkel, and J. Larsen (2005), Cosmogenically enabled sediment budgeting, *Geology*, *33*, 133–136.

Oskin, M., L. Perg, E. Shelef, M. Strane, E. Gurney, B. Singer, and X. Zhang (2008), Elevated shear zone loading rate during an earthquake cluster in eastern California, *Geology*, *36*, 507–510.

Paola, C., P. L. Heller, and C. L. Angevine (1992a), The large-scale dynamics of grain-size variation in alluvial basins, 1: Theory, *Basin Res.*, *4*, 73–90.

Paola, C., G. Parker, R. Seal, S. Sinha, J. Southard, and R. Wilcock (1992b), Downstream fining by selective deposition in a laboratory flume., *Science*, *258*, 1757–1760.

Parker, G., C. Paola, and S. Leclair (2000), Probabilistic Exner Continuity equation for mixture with no active layer, *J. Hydraul. Eng.*, *126*, 818–826.

Pyrce, R. S., and P. E. Ashmore (2003), The relation between particle path length distributions and channel morphology in gravel-bed streams: A synthesis, *Geomorphology*, *56*, 167–187.

Repka, J. L., R. S. Anderson, and R. C. Finkel (1997), Cosmogenic dating of fluvial terraces, Fremont River, Utah, *Earth Planet. Sci. Lett.*, *152*, 59–73.

Sklar, L., and W. Dietrich (2001), Sediment and rock strength controls on river incision into bedrock, *Geology*, *29*(12), 1087–1090.

Sklar, L., and W. Dietrich (2004), A mechanistic model for river incision into bedrock by saltating bed load, *Water Resour. Res.*, *40*, W06301, doi:10.1029/2003WR002496.

Sklar, L., and W. Dietrich (2006), The role of sediment in controlling steady-state bedrock channel slope: Implications of the saltationabrasion incision model, *Geomorphology*, *82*, 58–83, doi:10.1016/j.geomorph.2005.08.019.

Sklar, L., W. Dietrich, and E. William (2008), Implications of the saltation-abrasion bedrock incision model for steady-state river longitudinal profile relief and concavity, *Earth Surf. Processes Landforms*, *33*, 1129–1151, doi:10.1002/esp.1689.

Small, E., R. Anderson, and G. Hancock (1999), Estimates of the rate of regolith production using ^{10}Be and ^{26}Al from an alpine hillslope, *Geomorphology*, *27*, 131–150, doi:ISI:000078769000010.

Stark, C., and F. Guzzetti (2009), Landslide rupture and the probability distribution of mobilized debris volumes, *J. Geophys. Res.*, *114*, F00A02, doi:10.1029/2008JF001008.

Stark, C., and N. Hovius (2001), The characterization of landslide size distributions, *Geophys. Res. Lett.*, *28*, 1091–1094.

Stark, C., E. Foufoula-Georgiou, and V. Ganti (2009), A nonlocal theory of sediment buffering and bedrock channel evolution, *J. Geophys. Res.*, *114*, F01029, doi:10.1029/2008JF000981.

Stone, J. (2000), Air pressure and cosmogenic isotope production, *J. Geophys. Res.*, *105*, 23,753–23,759.

Tucker, G., and D. Bradley (2010), Trouble with diffusion: Reassessing hillslope erosion laws with a particle based model, *J. Geophys. Res.*, *115*, F00A10, doi:10.1029/2009JF001264.

Turowski, J., D. Lague, and N. Hovius (2007), Cover effect in bedrock abrasion: A new derivation and its implications for the modeling of bedrock channel morphology, *J. Geophys. Res.*, *112*, F04006, doi:10.1029/2006JF000697.

Turowski, J. M., E. M. Yager, A. Badoux, D. Rickenmann, and P. Molnar (2009), The impact of exceptional events on erosion, bedload transport and channel stability in a step-pool channel, *Earth Surf. Processes Landforms*, *34*, 1661–1673, doi:10.1002/esp.1855.

Vassallo, R., et al. (2007), Transpressional Tectonics and stream terraces of the Gobi-Altay, Mongolia, *Tectonics*, *26*, TC5013, doi:10.1029/2006TC002081.

Vericat, D., D. Church, and R. Batalla (2006), Bed load bias: Comparison of measurements obtained using two (76 and 152 mm) Helley-Smith samplers in a gravel bed river, *Water Resour. Res.*, *42*, W01402, doi:10.1029/2005WR004025.

Vigier, N., B. Bourdon, S. Turner, and J. Allègre (2001), Erosion timescales derived from U-decay series measurements in rivers, *Earth Planet. Sci. Lett.*, *193*, 549–563.

Whipple, K. X., and G. E. Tucker (1999), Dynamics of the stream-power incision model: Implication for height limits of mountain ranges, landscape response timescales, and research needs, *J. Geophys. Res.*, *104*, 17,661–17,674.

Whipple, K. X., and G. E. Tucker (2002), Implication of sediment-flux-dependent river incision models for landscape evolution, *J. Geophys. Res.*, *107*(B2), 2039, doi:10.1029/2000JB000044.

Whipple, K. X., G. S. Hancock, and R. S. Anderson (2000), River incision into bedrock: Mechanics and relative efficacy of plucking, abrasion and cavitation, *Geol. Soc. Am. Bull.*, *112*, 490–503.

Wilcock, P. R. (1997), The components of fractional transport rate, *Water Resour. Res.*, *33*, 247–258.

Witt, A., B. Malamud, M. Rossi, F. Guzzetti, and S. Peruccacci (2010), Temporal correlations and clustering of landslides, *Earth Surf. Processes Landforms*, *35*, 1138–1156.

Wittmann, H., F. von Blanckenburg, J. L. Guyot, L. Maurice, and P. W. Kubik (2009), From source to sink: Preserving the cosmogenic ^{10}Be-derived denudation rate signal of the Bolivian Andes in sediment of the Beni and Mamore foreland basins, *Earth Planet. Sci. Lett.*, *288*, 463–474, doi:10.1016/j.epsl.2009.10.008.

Yanites, B., G. Tucker, and R. Anderson (2009), Numerical and analytical models of cosmogenic radionuclide dynamics in landslide-dominated drainage basins, *J. Geophys. Res.*, *114*, F01007, doi:10.1029/2008JF001088.

S. Carretier and V. Regard, GET, UPS (SVT-OMP), Université de Toulouse, 14 Av. Edouard Belin, F-31400 Toulouse, France. (sebastien.carretier@get.obs-mip.fr)